

Reflection and emission of Brillouin zone edge states for active photonic crystal waveguides

A D Bristow^{1,4}, A García-Déniz¹, A M Fox¹, D M Whittaker¹,
M S Skolnick¹, T F Krauss² and M Hopkinson³

¹ Department of Physics and Astronomy, University of Sheffield, Sheffield, S3 7RH, UK

² School of Physics and Astronomy, University of St Andrews, St Andrews, KY16 9SS, UK

³ Department of Electronic and Electrical Engineering, University of Sheffield, Sheffield, S1 3JD, UK

E-mail: mark.fox@sheffield.ac.uk

Received 4 November 2004, accepted for publication 17 January 2005

Published 9 May 2005

Online at stacks.iop.org/JOptA/7/S270

Abstract

A one-dimensional photonic crystal is patterned into an active planar waveguide containing multiple InGaAs quantum wells. External coupling reflectivity is used to map out the photonic band structure, revealing a clear anti-crossing at ~ 1.37 eV in the 45° TM polarized spectrum. The band structure is compared to and confirmed by scattering-matrix calculations. Photoluminescence measurements are performed in the same geometry on the patterned and unpatterned regions of the sample. The latter shows conventional quantum-well emission and GaAs emission with increasing pump power. In contrast, the spectra from the patterned sample contain a sharp mode from the dielectric-like band of the anti-crossing, corresponding to the Brillouin zone edge. Power-dependent excitation shows this mode to be strongly super-linear, indicative of band edge lasing.

Keywords: photonic crystal, phase-matching, laser emission

1. Introduction

Since the advent of photonic crystals [1], periodically patterned materials have been demonstrated to control the propagation and emission of light. The periodic modulation of the refractive index leads to the formation of photonic band gaps, analogous to that of the electronic band gap in semiconductor crystals. The band gap is associated with a range of frequencies where light cannot propagate in the medium. Hence, if a radiative source is embedded into a patterned material, its emission is suppressed in this frequency range [2, 3]. Similarly, the emission from an embedded source can be enhanced by the bare photonic crystal [4, 5] or by introducing a defect into the lattice [6–8].

In the former case, locating the source at the edge of the band gap utilizes the increased density of optical states [9, 10].

⁴ Present address: Department of Physics, University of Toronto, Toronto, ON, M5S 1A7, Canada.

The dispersions of the photonic bands flatten towards the Brillouin zone edge and produce heavy photon states at their edge [11]; the semiconductor analogy is the increased effective mass of the carriers. Subsequently, strong modification of the material's effective refractive index can lead to phenomena such as enhanced refraction effects and beam steering [12–14]. This dramatically alters the propagation of light, allowing for strong light–matter interactions and the creation of optical gain or lasing action from embedded sources [15, 16].

A particular form of photonic crystal is the photonic crystal waveguide (PCW) [17], which employs planar waveguide confinement in the growth direction of the structure and band gap confinement in the plane of the waveguide. The single most important technological advantage of this class of photonic crystals is the transferability of growth and fabrication tools from the semiconductor industry. Consequently, it is straightforward to incorporate multiple quantum wells (MQWs) in the waveguide core which act as embedded

emitters [18]. More complex patterning can be achieved to include high- Q cavities from which lasing action has been seen and widely studied; see for example [8, 19]. However, there is much theoretical [20–23] and experimental [24, 25] interest in laser action from the photonic band structure that arises from bare or perfect crystal lattices.

In this paper, a one-dimensional (1D) PCW containing MQW emitters is investigated by means of angle-tuned external coupling reflectivity to determine the photonic band structure [26]. The photonic Brillouin zone edge is examined and the photonic band edge states are established. In conjunction with this, scattering-matrix calculations [27] are used to numerically model the structure; these show strong agreement with the experimental band structure. Photoluminescence (PL) measurements are then performed to examine the emission properties of the MQWs from within the structure for both the unpatterned and patterned waveguides. The bare waveguide shows strong luminescence from the excitons related to the MQWs at low power and also from the GaAs band edge at higher excitation powers. In contrast the patterned structure shows an extra feature at a wavelength that corresponds to the lower edge of the photonic band gap. The power-dependent PL for this mode shows a super-linear behaviour with a threshold indicative of lasing from the band edge states.

2. Experimental details

The PCW is based on an asymmetrical planar waveguide grown onto a GaAs substrate by molecular beam epitaxy (MBE). As shown in figure 1(A), the layer structure consists of a 400 nm core that contains seven ≈ 10 nm wide $\text{In}_{0.12}\text{Ga}_{0.88}\text{As}$ MQWs in GaAs surrounded by $\text{Al}_{0.3}\text{Ga}_{0.7}\text{As}$ barriers to prevent carriers escaping from the MQW region. The core layer sits on top of an 800 nm thick $\text{Al}_{0.6}\text{Ga}_{0.4}\text{As}$ lower cladding layer. The top cladding layer is air. In the figure the layer structure is represented with different shades; white denotes pure GaAs in the core and substrate, with light grey for the $\text{Al}_{0.3}\text{Ga}_{0.7}\text{As}$ barriers and dark grey for the $\text{Al}_{0.9}\text{Ga}_{0.1}\text{As}$ cladding. The $\text{In}_{0.12}\text{Ga}_{0.88}\text{As}$ MQWs in the centre of the core region are represented by dashed lines.

The active waveguide structure is then patterned by electron beam lithography and reactive ion etching from the top surface. The sample of interest to us in this paper has a 1D grating etched through part of the waveguide structure. The etch depth is approximately 100 nm, leaving the MQWs intact. The 1D lattice of air trenches has a period of 530 nm and an air fill factor of $\sim 15\%$. A scanning electron microscope (SEM) is used to verify sample quality; see figure 1(B).

Linear reflection measurements are performed to characterize the photonic band structure of the 1D PCW sample. The experimental apparatus is described in detail elsewhere [28]. In brief, a white-light spectrum from a tungsten-halogen lamp is collimated with an angular divergence of $< 1^\circ$ and is linearly polarized with either transverse electric (TE) or transverse magnetic (TM) polarization; see figure 1(A). This light is then specularly reflected off the surface of the sample, such that it has an in-plane component of the k -vector (k_{\parallel}) that can phase match to the photonic modes of the PCW. The phase-matching condition

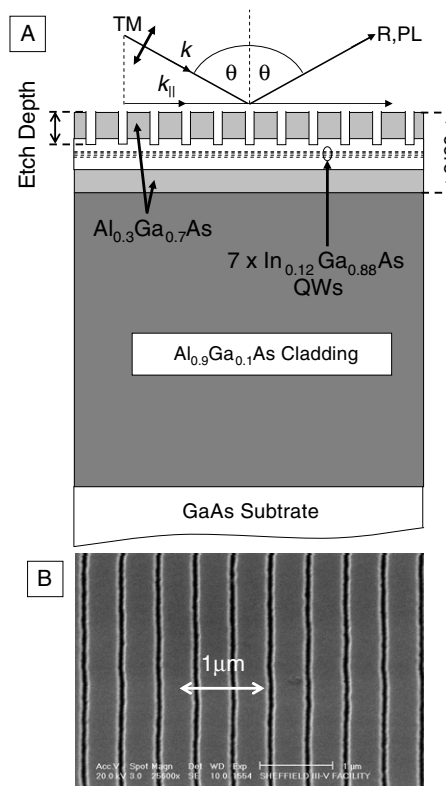


Figure 1. (A) A labelled schematic diagram of the layer structure patterned with a shallowly etched photonic lattice. Above the structure the experimental geometry for both the reflectivity and the photoluminescence measurements is shown. (B) A surface-view scanning electron micrograph of the 1D photonic lattice.

can be adjusted by the angle of incidence (θ), which is related to the in-plane k -vector by the relationship $k_{\parallel} = (\omega/c) \times \sin(\theta)$, where ω is the angular frequency of the incident radiation and c is the speed of light in vacuum. The reflected light is coupled into a spectrometer which has a liquid N_2 cooled Ge detector, allowing for acquisition of angle-tuned reflectivity spectra.

The PL measurements were performed with a 1 kHz pulsed Ti:sapphire regenerative amplifier with a wavelength of 800 nm and a pulse width of 130 fs. Consequently, the intense laser beam can be split into several beams, one of which was used to perform spectroscopy with a white-light continuum [29] generated in a 3 mm piece of polished sapphire. The details for this *in situ* reflectivity are also given elsewhere [30]. The technique is suitable for quickly determining smaller regions of the photonic band structure. The method of acquisition requires a balanced detection system to stabilize inherent fluctuations and the strong wavelength dependence of the white-light continuum. This is achieved by using a charge-coupled device (CCD) attached to a spectrometer and coupling the reflected beam and a reference beam into them. Vertical separation of the beams on the CCD chip and binning the read-out such that the reference and signal traces can be separated gives the possibility of removing the background in real time.

The *in situ* reflectivity is useful for verification of the photonic modes to be investigated by means of PL *in situ*, i.e. away from the linear reflectivity set-up discussed in detail previously. This is important for instant feedback

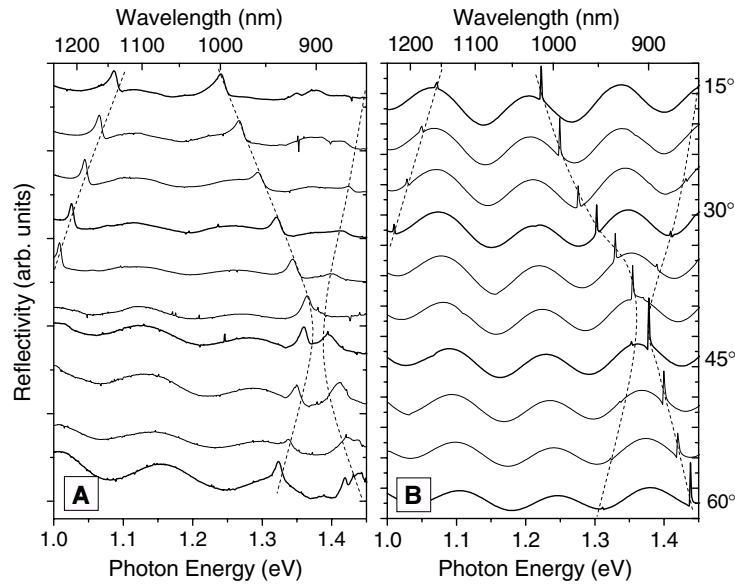


Figure 2. (A) Experimental and (B) theoretical external coupling reflectivity spectra for TM polarization. The incident and reflection angles are simultaneously varied over the range $15^\circ \leq \theta \leq 60^\circ$ in 5° steps. Dashed construction lines are used to show the dispersion of the observed photonic coupling modes.

on calibration of wavelength, polarization and angle of incidence of the modes to be examined. Also, this method provides information about the integrity of the structure after performing PL measurements. This is critical since the light source employed is a high intensity laser, capable of damaging the semiconductor and the photonic crystal structure catastrophically.

The remainder of the laser beam (which is not used for the *in situ* reflectivity) is then attenuated appropriately for PL measurements. The laser light excites the sample with a photon energy that exceeds the interband transition energy of the InGaAs MQWs and the GaAs materials in the structure. The focused spot diameter of the pump beam is $<200 \mu\text{m}$, compared to the sample area of $80 \mu\text{m} \times 80 \mu\text{m}$. The angle of excitation is arbitrarily chosen to be smaller than the angle of incidence for the *in situ* reflectivity. Power-dependent measurements are obtained by varying the incident power with a graded neutral density filter wheel. All measurements presented here are performed at room temperature. Furthermore, since the TE modes were less well resolved than the TM modes, we only report here the results of *in situ* reflectivity and PL measurements for TM polarization. In principle, band edge lasing should also be possible for TE polarization, provided that well-defined modes that are nearly resonant with the MQW PL can be engineered.

3. External coupling reflectivity

Figure 2(A) shows a typical set of reflectivity spectra for this 1D PCW. The angular range is $15^\circ \leq \theta \leq 60^\circ$ in 5° steps and the incident beam of light is TM polarized. The spectra show a weak oscillating background arising from the Fabry–Perot interference in the vertical direction of the waveguide, on top of which are superimposed several sharp coupling features which correspond to leaky modes of the photonic band structure. There are three distinct bands which can be deduced from

the angle-dependent reflectivity spectra (indicated by dashed lines). Of importance are the upper two bands, which undergo an anti-crossing close to 45° and correspond to a photonic band gap between $1.35 \text{ eV} \leq E \leq 1.39 \text{ eV}$. The anti-crossing behaviour occurs at the photonic Brillouin zone edge, and modes on either side of it can be either described as *air band-like* or *dielectric band-like*. The bands are separated in energy because their in-plane field distribution is either strongly aligned with the air or with the semiconductor regions of the lattice, respectively [9]. The result is a lifting of the degeneracy of modes in adjacent bands at the Brillouin zone edge and creation of the band gap.

Numerically simulated reflectivity spectra are shown in figure 2(B) for the same conditions as for the experiment. The simulations are performed by means of scattering-matrix calculations [27] and are designed to incorporate the coupling of the external radiation field to the modes of the patterned multilayer structure. The initial simulation parameters are obtained from the wafer growth and the SEM of the patterned lattice. In the model the MQW region is simulated by a slight adjustment of the refractive index of the GaAs within the core layer of the waveguide. Nonetheless, there is very good agreement between the theoretical spectra and those obtained from experiment.

The culmination of the experimental spectra for both TE and TM polarized light is a photonic band structure, shown in figure 3. The photonic band structure is plotted such that it highlights the angle dependence of the reflectivity measurement over the range from 15° to 60° . The grey region is marked for the TM band gap, which will be useful in the following discussion for the emission properties of the patterned wafer. From the figure it becomes clear that the edge of the Brillouin zone at $k_{\parallel} = \pi/a$ (dotted line) intersects the anti-crossing observed from the reflectivity spectra corresponding to $\theta = 45^\circ$. Consequently, the PL measurements will be performed for this angle and verified by the *in situ* reflectivity.

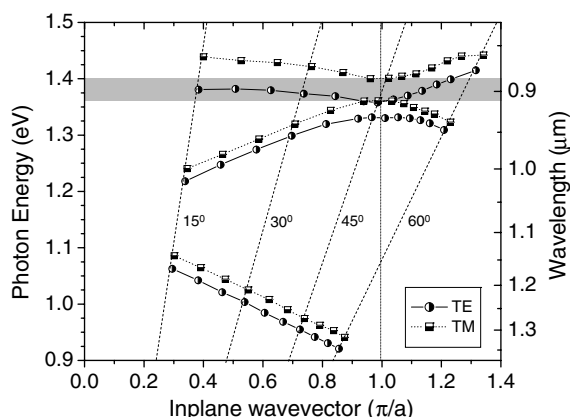


Figure 3. The photonic band structure extracted from the reflection spectra, showing both TE and TM polarization. The TM polarized band gap is marked in grey. For this period, $a = 530$ nm, the Brillouin zone edge π/a is indicated by a dotted vertical line and the 15° increments of the angle θ are marked by dashed lines.

4. Photoluminescence spectroscopy

Using the white-light continuum from the Ti:sapphire amplifier, an *in situ* reflectivity measurement was performed at 45° with TM polarization to ensure the correct positioning of the band edge coupling resonances, shown in figure 4(A). Two features are observed at 895 and 916 nm, matching the band edge features mapped out in the angle-dependent reflectivity measurements performed earlier.

The white-light continuum was then blocked and the 800 nm pump beam excited the sample at an angle of incidence of $<30^\circ$. In this geometry the PL emitted from the wafer at $\theta = 45^\circ$ can be examined using the same collection optics as for the *in situ* reflectivity measurement. The PL is measured for both the unpatterned and patterned regions of the semiconductor wafer; see figures 4(B) and (C), respectively. For these two plots the excitation beam has an average pump power of $\sim 300 \mu\text{W}$. The comparison of these three plots highlights the interesting features that arises from the combination of the active semiconductor waveguide and from the photonic lattice. The bare wafer has emission corresponding to the MQWs at ~ 1.32 eV. This emission is only very weakly angle dependent, so that effect is ignored here. For the patterned structure the 45° emission exhibits an additional feature at ~ 1.35 eV corresponding to one of the band edge resonances that was of interest in our reflectivity measurements. The existence of one single band edge feature in the PL will be discussed below. In figure 4(C) the MQW emission can also be seen along with a large amount of background radiation from the waveguide structure; also noted is the band edge of the pure GaAs at $E_g = 1.42$ eV at room temperature.

The presence of strong background emission across the spectral region of interest requires a study of the power dependence of the PL, shown in figure 5. The emission spectra from the unpatterned region of the wafer are presented for a range of average powers, $50 \mu\text{W} \leq P_{\text{ave}} \leq 4$ mW. At lower powers only the room temperature exciton emission associated with the MQWs can be seen. For increasing powers the emission spectra become more complicated: the lower energy states become saturated leading to emission from higher

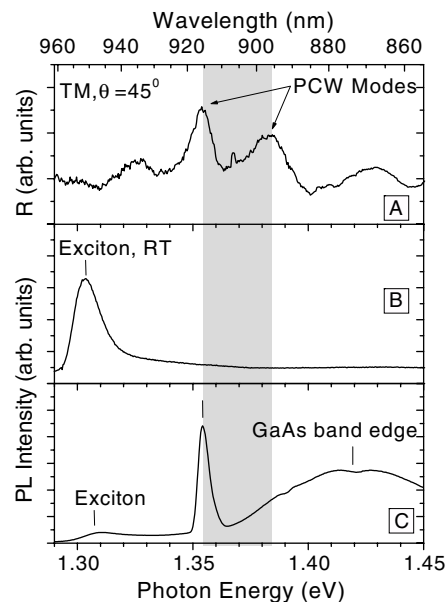


Figure 4. (A) *In situ* reflectivity spectra measured with the white-light laser continuum for $\theta = 45^\circ$ and TM polarization. Photonic coupling modes are observed at 896 and 915 nm. (B) Photoluminescence spectra from the unpatterned wafer showing the exciton peak associated with the InGaAs quantum wells at room temperature. (C) Photoluminescence from the patterned region of the wafer showing the exciton peak from (B), the luminescence from the pure GaAs and a strong sharp mode at ~ 1.355 eV (915 nm). A dashed vertical line indicates the similarity in position of the feature in the reflection and photoluminescence spectra. The grey region represents the photonic band gap.

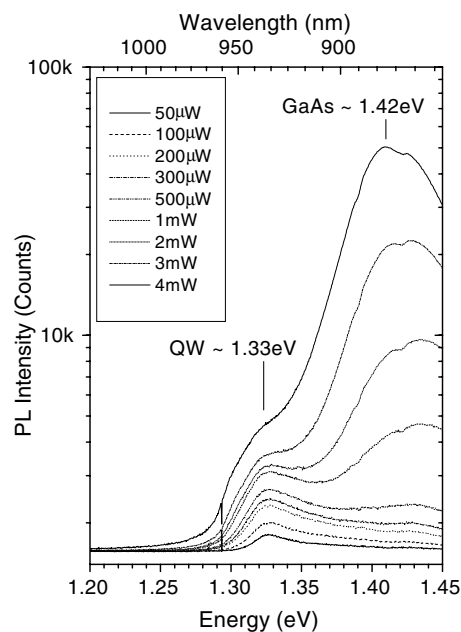


Figure 5. Power-dependent PL spectra from the unpatterned wafer at $\theta = 45^\circ$. The average pump power is varied over the range $50 \mu\text{W} \leq P_{\text{ave}} \leq 4$ mW.

states in the MQW, also the continuum of states in the GaAs layers surrounding them become populated and begin to emit. However, over the wavelength range of interest, the power-dependent response of any particular feature would show a

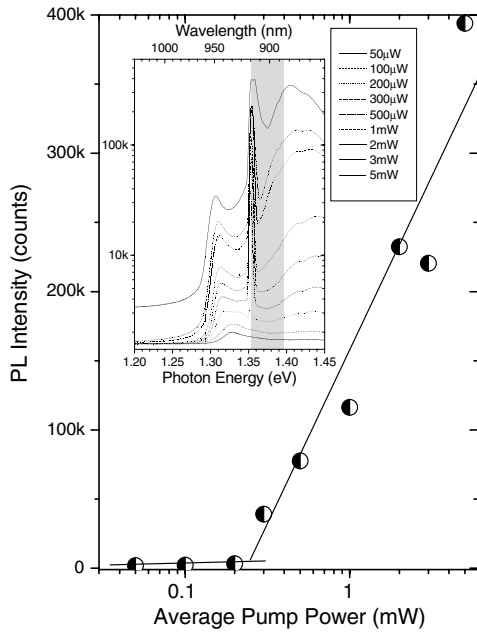


Figure 6. The power-dependent response of the photonic feature at 1.355 eV, showing a nonlinear increase in the peak luminescence of the leaky mode. The inset shows the power-dependent photoluminescence spectra from the patterned sample for the range of average pump powers $50 \mu\text{W} \leq P_{\text{ave}} \leq 5 \text{ mW}$. The grey region represents the photonic band gap.

linear increase with the intensity of the excitation beam. It should also be noted that at higher pump powers a red-shift of the spectral features is observed. The intense laser source introduces a large carrier density (up to $\sim 10^{19} \text{ cm}^{-3}$) in the structure, leading to a heating effect that decreases the electronic band gap of the material.

The emission from the patterned region of wafer has many similar features and one striking exception compared to that from the bare wafer; see the inset of figure 6. From the discussion of figure 4(B) and (C) the band edge feature at $\sim 1.35 \text{ eV}$ is also of most interest in the power dependence presented here. The results of the PL study of the unpatterned wafer explain the background in the figure inset and will not be considered for now. The spectra presented here are for the average pump power range $50 \mu\text{W} \leq P_{\text{ave}} \leq 5 \text{ mW}$. In the main part of figure 6, the peak emission intensity of the $\sim 1.35 \text{ eV}$ feature is plotted against average power on a semi-log scale. As the power is increased the intensity is linear up to 0.2 mW, where a clear threshold is observed, above which the mode is strongly super-linear. The increase in the gradient is approximately by two orders of magnitude, due to a strong amplification of the emission of $\sim 40 \text{ meV}$ above the room temperature excitons in the MQWs.

Above threshold the quality factor of the $\sim 1.35 \text{ eV}$ mode is $Q = \lambda/\Delta\lambda \simeq 300$, which is resolution limited due to the large background emission. Nonetheless, this is not a particularly large value for a lasing mode. However, the width of photonic bands is of the order of 10 meV which would result in a smaller value of Q than that observed here. Furthermore, these time averaged spectra are expected to be affected by the nonlinear absorption and a change in the refractive index of the material induced by the strength of the PL source [30].

This would result in a shift of the photonic bands leading to broadening in a time averaged measurement. At higher powers the broadening of the photonic mode does indeed increase and consequently the Q -factor goes down, supporting the hypothesis that increased broadening is occurring due to increased multiphoton absorption and a larger nonlinear shift of the photonic mode [31].

The observed threshold is believed to be the onset of band edge lasing and is expected for only one of the two band Brillouin zone edge resonances. This can be explained by the in-plane distribution of the field for the mode under investigation. As discussed above, bands on either side of the gap can be either dielectric band-like or air band-like. The mode on the lower side of the gap is dielectric band-like. Consequently, the modes associated with dielectric-like bands are more suitable for lasing due a larger overlap of the light with the active material embedded in the structure. This mode is characterized by having most of the electromagnetic energy inside the dielectric region of the unit cell of the photonic lattice and is verified by scattering-matrix simulations for the in-plane electromagnetic energy density.

The value of the threshold observed here is relatively high, but we expect lower thresholds to be obtainable by optimizing the design. This could be achieved, for example, by using MQWs with an indium concentration of approximately 8% for the same photonic lattice, or by reducing the period of the photonic lattice by $\sim 35\%$ for the same MQWs. Either method would lead to resonant coupling of the MQW emission to the dielectric band-like modes associated with the band edge. This would probably reduce the onset of the lasing, therefore improving the threshold. Moreover, we would also expect the lasing threshold to decrease as more perfect photonic crystals with fewer structural imperfections become available.

5. Conclusion

In conclusion, the patterning of a 1D photonic lattice produces a photonic band structure that is readily observable by means of external coupling reflectivity. At the photonic Brillouin zone the dispersion is flattened and longer light-matter interaction times gives rise to the band edge lasing phenomenon. Observed here is a strong nonlinear power dependence of the mode on a dielectric band, corresponding to lower energy side of the photonic band gap.

Acknowledgments

This work was funded by the EPSRC grants GR/M72951 and GR/M22529.

References

- [1] Yablonovich E 1987 Inhibited spontaneous emission in solid-state physics and electronics *Phys. Rev. Lett.* **58** 2059
John S 1987 Strong localization of photons in certain disordered dielectric superlattices *Phys. Rev. Lett.* **58** 2486
- [2] Romanov S G, Maka T, Sotomayor Torres C M, Müller M and Zentel R 2002 Suppression of spontaneous emission in incomplete opaline crystals *J. Appl. Phys.* **91** 9426
- [3] Yoshino K, Lee S B, Tatsuhara S, Kawagishi Y, Ozaki M and Zakhidov A A 1998 Observation of inhibited spontaneous emission and stimulated emission of rhodamine 6G in polymer replica of synthetic opal *Appl. Phys. Lett.* **73** 3506

- [4] Vlasov Y A, Luterova K, Pelant I, Hönerlage B and Astratov V N 1997 Enhancement of optical gain of semiconductors embedded in three-dimensional photonic crystals *Appl. Phys. Lett.* **71** 1616
- [5] Romanov S G, Maka T, Sotomayor Torres C M, Müller M and Zentel R 1999 Photonic band-gap effects upon the light emission from a dye-polymer-opal composite *Appl. Phys. Lett.* **75** 1057
- [6] Foresi J S, Villeneuve P R, Ferrera J, Thoen E R, Steinmeyer G, Fan S, Joannopoulos J D, Kimerling L C, Smith H I and Ippen E P 1997 Photonic-bandgap microcavities in optical waveguides *Nature* **390** 6656
- [7] Benisty H *et al* 1999 Optical and confinement properties of two-dimensional photonic crystals *J. Lightwave Technol.* **17** 2063
- [8] Painter O J, Husain A, Scherer A, O'Brien J D, Kim I and Dapkus P D 1999 Room temperature photonic crystal defect lasers at near-infrared wavelengths in InGaAsP *J. Lightwave Technol.* **17** 2082
- [9] Joannopoulos J D, Meade R D and Winn J N 1995 *Photonic Crystal* (Princeton, NJ: Princeton University Press)
- [10] Sakoda K 1999 Enhanced light amplification due to group-velocity anomaly peculiar to two- and three-dimensional photonic crystals *Opt. Express* **4** 167
- [11] Astratov V N, Stevenson R M, Culshaw I S, Whittaker D M, Skolnick M S, Krauss T F and De La Rue R M 2000 Heavy photon dispersions in photonic crystal waveguides *Appl. Phys. Lett.* **77** 178
- [12] Halevi P, Krokhin A A and Arriga J 1999 Photonic crystals as optical components *Appl. Phys. Lett.* **75** 2725
- [13] Kosaka H, Kawashima T, Tomita A, Notomi M, Tamamura T, Sato T and Kawakami S 1999 Self-collimating phenomena in photonic crystals *Appl. Phys. Lett.* **74** 1212
- Kosaka H, Kawashima T, Tomita A, Notomi M, Tamamura T, Sato T and Kawakami S 1999 Photonic crystals for micro lightwave circuits using wavelength-dependent angular beam steering *Appl. Phys. Lett.* **74** 1370
- [14] Enoch S, Tayeb G and Maystre D 1999 Numerical evidence of ultrarefractive optics in photonic crystals *Opt. Commun.* **161** 171
- [15] Ohtaka K 1999 Density of states of slab photonic crystals and the laser oscillation in photonic crystals *J. Lightwave Technol.* **17** 2161
- [16] Andrew P, Turnbull G A, Samuel I D W and Barnes W L 2002 Photonic band structure and emission characteristics of a metal-backed polymeric distributed feedback laser *Appl. Phys. Lett.* **81** 954
- [17] Krauss T F, De La Rue R M and Brand S 1996 Two-dimensional photonic-bandgap structures operating at near-infrared wavelengths *Nature* **383** 699
- [18] van der Ziel J P, Dingle R, Miller R C, Weigmann W and Nordland W A Jr 1975 Laser oscillation from quantum states in very thin GaAs-Al_{0.2}Ga_{0.8}As multilayer structures *Appl. Phys. Lett.* **26** 463
- [19] Srinivasan K, Barclay P, Painter O, Chen J, Cho A Y and Gmachl C 2003 Experimental demonstration of a high quality factor photonic crystal microcavity *Appl. Phys. Lett.* **83** 1915
- [20] Nojima S 2001 Optical-gain enhancement in two-dimensional active photonic crystals *J. Appl. Phys.* **90** 545
- [21] Lousse V, Vigneron J-P, Bouju X and Vigoureux J-M 2001 Atomic radiation rates in photonic crystals *Phys. Rev. B* **64** R201104
- [22] Florescu L, Busch K and John S 2002 Semiclassical theory of lasing in photonic crystals *J. Opt. Soc. Am. B* **19** 2215
- [23] Xu X S, Cheng B Y and Zhang B Z 2003 Transient gain in photonic crystals *Appl. Phys. B* **77** 515
- [24] Susa N 2001 Threshold gain and gain enhancement due to distributed-feedback in two-dimensional photonic-crystal lasers *J. Appl. Phys.* **89** 815
- [25] Kwon S H, Ryu H Y, Kim G H, Lee Y H and Kim S B 2003 Photonic bandedge lasers in two-dimensional square-lattice photonic crystal slabs *Appl. Phys. Lett.* **83** 3870
- [26] Astratov V N, Stevenson R M, Skolnick M S, Whittaker D M, Brand S, Culshaw I S, Krauss T F, De La Rue R M and Karimov O Z 1998 Experimental technique to determining the band structure of two-dimensional photonic lattices *IEEE Proc. Optoelectron.* **145** 398
- [27] Whittaker D M and Culshaw I S 1999 Scattering-matrix treatment of patterned multilayer photonic structures *Phys. Rev. B* **60** 2610
- [28] Bristow A D, Astratov V N, Shimada R, Culshaw I S, Whittaker D M, Skolnick M S, Tahraoui A and Krauss T F 2002 Polarization conversion in the reflection properties of photonic crystal waveguides *IEEE J. Quantum Electron.* **38** 880
- [29] Fork R L, Shank C V, Hirlimann C, Yen R and Tomlinson W J 1983 Femtosecond white-light continuum pulses *Opt. Lett.* **8** 1
- [30] Bristow A D, Wells A-P R, Fan W H, Fox A M, Skolnick M S, Whittaker D M, Tahraoui A, Krauss T F and Roberts J S 2003 Ultrafast nonlinear response of AlGaAs two-dimensional photonic crystal waveguides *Appl. Phys. Lett.* **83** 851
- [31] Bristow A D, Kundys D O, García-Déniz A Z, Wells A-P R, Fox A M, Skolnick M S, Whittaker D M, Tahraoui A, Krauss T F and Roberts J S 2004 Ultrafast nonlinear tuning of the reflection properties of AlGaAs photonic crystal waveguides by two-photon absorption *J. Appl. Phys.* **96** 4729